Journal of Catalysis **187,** 436–452 (1999)
Article ID jcat.1999.2638, available online at http://www.idealibrary.com on IDEAL®

Active and Spectator Adsorbates during NO Decomposition over Cu–ZSM-5: Transient IR, Site-Poisoning, and Site-Promotion Studies

Mahesh V. Konduru and Steven S. C. Chuang[1]

Department of Chemical Engineering, The University of Akron, Akron, Ohio 44325-3906

Received April 9, 1999; revised July 6, 1999; accepted July 17, 1999

A site-poisoning and -promotion technique was employed to investigate the role of adsorbates and to formulate a reaction pathway for the NO decomposition reaction over Cu–ZSM-5. Transient infrared and mass spectrometer studies of pulse NO reaction on under- and over-exchanged Cu–ZSM-5 reveal $Cu^{2+}(NO)$, $Cu^{+}(NO)$, bridging $Cu^{2+}(NO_3^-)$, and NO^+ as the major adsorbates and N_2, N_2O, O_2, and NO_2 as the products. SiH_4 and H_2O moderately inhibited $Cu^{+}(NO)$ and N_2 formation, but severely inhibited $Cu^{2+}(NO_3^-)$ and O_2 formation. Addition of CO as a reducing agent led to the promotion of Cu^{2+} reduction to Cu^{+}, depletion of $Cu^{2+}(NO_3^-)$, increase in NO conversion and O_2 formation as well as formation of CO_2. These results revealed that N_2 and O_2 formation proceeds through separate rate-limiting steps; O_2 formation occurs via both autoreduction of Cu^{2+} to Cu^{+} and decomposition of $Cu^{2+}(NO_3^-)$. The results from pulse reaction studies on deactivated Cu–ZSM-5 reveal that O_2 formation is more sensitive to poisoning than NO dissociation and N_2 formation. Although silanation may improve the hydrothermal stability of the catalyst, silanation severely inhibited O_2 and $Cu^{2+}(NO_3^-)$ formation through inhibition of adsorbed O migration. Promotion of O_2 desorption by addition of a small amount of reducing agent such as CO in the presence of NO ($NO/CO > 3.5$) can greatly enhance NO decomposition activity. Further investigation is needed to study such an effect on the NO decomposition activity under the O_2 environment.

Key Words: **site poisoning; site promotion; *in situ* IR; direct NO decomposition; Cu–ZSM-5; over-exchanged; under-exchanged; active adsorbates; spectator adsorbates; reaction mechanism; deactivation pathway; CO promotion.**

INTRODUCTION

In situ infrared (IR) is one of the few techniques that allows observation of adsorbates, including the active and spectator species, under reaction conditions (1, 2). To distinguish the active adsorbates from spectator adsorbates, transient IR techniques with variation of reactant partial pressure and isotope composition have been used (3–9). Due to the rapid exchange between gaseous reactants and adsorbates, information obtained solely from transient IR techniques does not allow unambiguous identification of active and spectator adsorbates.

The present study reports the use of the transient IR technique coupled with site poisoning and CO site promotion to distinguish between active and spectator adsorbates from the IR-observable adsorbates during NO decomposition on under- and over-exchanged Cu–ZSM-5. NO decomposition over Cu–ZSM-5 was selected as the model reaction as (i) Cu–ZSM-5 exhibits high NO decomposition activity (10–19) and (ii) the structure of adsorbates on the Cu–ZSM-5 catalyst has been well established, but their reactivity not yet completely determined. Mechanistic information on the adsorbates' role in the reaction allows verification of various proposed NO decomposition mechanisms, unravels the limitation of Cu–ZSM-5 catalysts for NO decomposition, and guides catalyst development.

NO adsorbs as $Cu^{+}(NO)$ (1814 cm^{-1}), $Cu^{2+}(NO)$ (1910 cm^{-1}), $Cu^{2+}O^{-}(NO)$ (1895 cm^{-1}), $Cu^{+}(NO)_2$ (1733 and 1835 cm^{-1}), adsorbed NO^+ (2124 cm^{-1}), and NO_x ($x = 2$ or 3) species (1624, 1601, 1575, and 1315 cm^{-1}) over Cu–ZSM-5 at temperatures ranging from 77 to 298 K and pressures from 0.07 to 39.9 Torr of NO (13–21). NO adsorption at higher temperatures (>373 K) produced low-intensity IR-observable adsorbates. Exposure of Cu–ZSM-5 to 6090 ppm of NO at 573 K resulted in the appearance of weaker $Cu^{+}(NO)$ and $Cu^{2+}(NO)$ as well as stronger NO_x ($x = 2$ or 3) (1500–1624 cm^{-1} region) species compared to those at room temperature (13).

The band assignment for the NO_x species has been uncertain despite numerous NO adsorption IR studies (13–15, 18, 20–22). The classical assignment of the nitrato- (M–NO_3 where M is a metal ion) and nitro- (M–NO_2) complexes has been discussed in earlier studies (23–26). Bands above 1600 cm^{-1} were assigned to bridging nitrato species, those below 1600 cm^{-1} to chelating bidentate nitrato species, and those below 1500 cm^{-1} to nitrito and nitro species (24, 25). The present study follows the classical band assignment: the band at 1624 cm^{-1} is assigned to the bridging nitrato species and the band at 1575 cm^{-1} to the chelating nitrato species.

[1] To whom all the correspondence should be addressed. E-mail: schuang@uakron.edu.

0021-9517/99 $30.00

The role of the adsorbate species in the NO decomposition reaction needs to be identified to support the proposed reaction mechanisms. Since active sites bond the active adsorbates and catalyze their reactions, blocking active sites should inhibit the formation of active adsorbates and products. Water (H_2O) and sulfur dioxide (SO_2) are known to poison the Cu–ZSM-5 catalyst for the NO decomposition reaction (27). It is expected that these species would block the active sites that chemisorb the active adsorbates. Although H_2O and SO_2 may also block the sites that adsorb spectator adsorbate species, the adsorbates observed on the poisoned catalyst must be adsorbed on the sites that are not directly blocked by the poisons. These types of adsorbates are classified as spectators in this study. Silane (SiH_4) treatment of zeolites, leading to the depletion of surface hydroxyl groups, rendered the zeolites thermal- and water-resistant (28). Pretreating Cu–ZSM-5 with SiH_4 would provide hydrothermal stability to the catalyst system. The investigation of adsorbate behavior on the SiH_4-treated catalyst would allow the determination of the extent of SiH_4 modification on the NO decomposition activity. Surprisingly, SiH_4 treatment, which was expected to impart hydrothermal stability to the Cu–ZSM-5 catalyst, in fact poisoned the NO decomposition activity as shown in the present study. The poisoning of NO decomposition activity by silane, along with that by water and sulfur dioxide, was utilized for the identification of spectator and active adsorbates during NO decomposition over Cu–ZSM-5.

In addition to site blocking, the interconversion of Cu^+ and Cu^{2+} sites during NO decomposition over Cu–ZSM-5 may be controlled by the addition of a reducing agent. The reducing agent may accelerate the reduction of Cu^{2+} to Cu^+, thus affecting the concentration of the adsorbed species on the catalyst surface and promote NO conversion. CO was used as the reducing agent to promote NO conversion on Cu–ZSM-5 because of its reducing capability and distinctive vibrational frequency.

The main objective of this study is to shed new light into the dynamic behavior of adsorbates during the NO decomposition reaction over Cu–ZSM-5 sites poisoned by water, silane, and sulfur dioxide as well as sites promoted by CO. Identification of the adsorbates' role on the silane-, water-, and sulfur dioxide-poisoned catalyst could reveal active and spectator adsorbates as well as explain the site-deactivation and NO decomposition mechanisms.

EXPERIMENTAL

Catalyst Preparation

Copper-exchanged ZSM-5 catalysts with different Cu loadings were used in the present study. The under-exchanged Cu–ZSM-5, labeled Cu–ZSM-5-83, with 83% copper exchange was prepared by Johnson Matthey and supplied by the Catalyst Bank of Sandia National Laboratories. The over-exchanged Cu–ZSM-5, labeled Cu–ZSM-5-127, with a 127% copper exchange was prepared by repeated ion exchange of Cu–ZSM-5-83 in a 0.07 M copper acetate solution at a pH of 7. The amount of copper exchanged is defined as 2 times the ratio of copper and aluminum present in the catalyst sample (27). The catalyst samples were analyzed using inductively coupled plasma (ICP) emission spectroscopy (Galbraith Lab., Inc., Knoxville, TN 37921-1750) and their composition is listed in Table 1. The Cu–ZSM-5-83 catalyst was characterized by X-ray diffraction (XRD) and its XRD pattern closely resembled that of ZSM-5 (29).

TABLE 1

Composition of the Cu–ZSM-5 Catalysts Used in the Present Study

	Cu–ZSM-5-83	Cu–ZSM-5-127
Si/Al	24.4	24.4
Cu/Al	0.415	0.675
% Copper exchange	83	127

Pulse Reaction Studies

Three self-supporting disks of Cu–ZSM-5 (without KBr as diluent), each of 25 mg, were pressed by a hydraulic press at a pressure of 4000–4500 psi. One of the disks was placed in the IR beam path in the reactor cell (30) and the two other disks were broken down into flakes and placed in close vicinity of the self-supporting disk in the reactor outlet. The additional catalyst, in the reactor outlet, was added to increase the conversion of nitric oxide and to obtain a strong signal for the reactor effluent analysis by the mass spectrometer (MS). Prior to the pulse reaction studies, the Cu–ZSM-5 catalysts were autoreduced in flowing He at 773 K for 2 h in the *in situ* IR cell. The pulse reaction study, illustrated in Fig. 1, involved the use of a six-port gas chromatograph (GC) sample injection valve (Valco Instruments Co. Inc.) for the introduction of 1 cm^3 of NO into He, flowing at 45 cm^3/min over the catalyst. Pulse reaction studies were carried out before and after site poisoning to determine the adsorbate behavior and concentration of the reactor effluent with a Fourier transform infrared spectrometer (FTIR) and MS, respectively. A QMG 112 A (Balzers-Pfeiffer) MS was used to monitor the reactor effluent responses for studies over Cu–ZSM-5-83 and a Pfeiffer Prisma QMG 200 (Pfeiffer Vacuum Technology) MS was used for studies over Cu–ZSM-5-127. Calibration factors for each gaseous species were obtained by pulsing known amounts of gases into both the mass spectrometers. The MS profiles of each of the reactor effluent species were

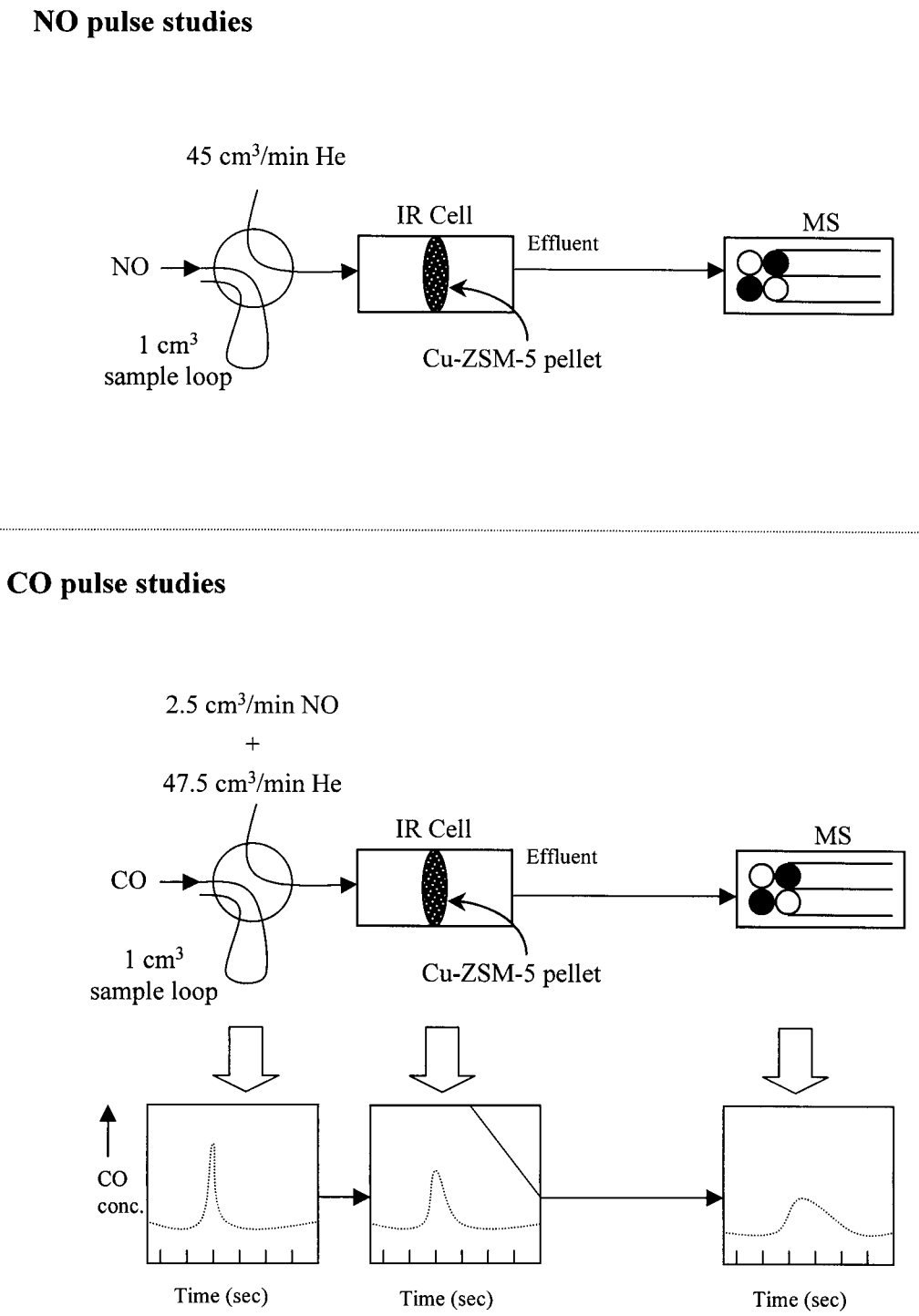

FIG. 1. Experimental setup during NO pulse and CO pulse reaction studies; the dashed pulse responses indicate the change in duration times due to spreading.

converted to their respective rate profiles with the help of the calibration factors. MS intensity profiles of NO_2 are presented instead of the rate profiles, as the calibration factor for NO_2 could not be obtained due to the lack of reliable NO_2 calibration gas and a low response factor. Although N_2O and NO_2 formation contributes to the intensity of NO ($m/e = 30$), such a contribution is of the order of $\pm 2\%$ due to the combination of low response factors for N_2O and NO_2 and low NO conversions obtained in the present study.

Site Poisoning

Autoreduced Cu–ZSM-5 samples, which exhibited pulse NO decomposition activity at 673 K, were site-poisoned by three kinds of pretreatment: (i) water treatment; (ii) silane treatment; and (iii) sulfur dioxide treatment. Water treatment (i.e., poisoning) involved exposure of the catalyst to steam at 773 K for 1 h. Silane treatment involved (i) CO adsorption on Cu^+/Cu^{2+} sites at 303 K to avoid the interaction between Cu^+/Cu^{2+} sites and silane, (ii) exposure of the CO-adsorbed catalyst to 1% SiH_4 in He flow at 303 K for 5 min, and (iii) maintenance of the reactor under batch conditions for 1 h at 373 K. Sulfur dioxide treatment involved exposure of the catalyst to 0.1% SO_2 in N_2 at 373 K for 1 h. Prior to each pulse reaction study, the site-poisoned catalysts were raised to the required temperatures in He flow.

The introduction of water, silane, and sulfur dioxide into the reactor cell was monitored by collecting the background spectra of the catalyst surface before and after the pretreatment. The exposure of the catalyst to water, silane, and sulfur dioxide was verified by infrared observation of these species in the IR cell.

Site Promotion

Promotion of copper sites on Cu–ZSM-5, for increase in NO conversion, involved pulsing 1 cm^3 of CO into a 5% NO in He flow (2.5 cm^3/min in 50 cm^3/min) over autoreduced Cu–ZSM-5-127 at 673 K. Prior to and during the introduction of the 1 cm^3 of CO, the autoreduced Cu–ZSM-5-127 sample was continuously exposed to a 5% NO in He flow as shown in Fig. 1. The 1 cm^3 of CO pulse was introduced into the 5% NO flow with a six-port GC sample injection valve. A Nicolet Magna 550 FTIR and the PRISMA MS recorded variation of adsorbate intensity and gaseous reactor effluent profiles during the CO pulse studies, respectively.

Spreading of Reactant Pulse

Figure 1 illustrates a reactant pulse input, introduced in a small amount of time (1.3 s), spreading as it moves along the length of a flow reactor due to turbulent mixing, velocity profile, and molecular diffusion effects (34). The extent of spreading can be characterized by the dispersion number (34). To avoid confusion with the term dispersion, used commonly to denote the metal crystal dispersion on a catalyst support, we use the term spreading in this study. The spreading of the pulse input leads to different time durations of the pulse at different positions along the reactor, as depicted in the case of the 1 cm^3 of CO pulse input, in dashed lines, in Fig. 1. Correlating the adsorbate behavior from the IR spectra and gaseous MS profiles requires accounting for these differences in the time duration of the 1 cm^3 pulse. The time duration difference can be corrected in the case of reactions involving components that display gas phase in both the IR spectra and MS profiles. For example, pulsing 1 cm^3 of CO into 5% NO flow produced CO_2, observed in both FTIR and MS, allowing adjustment of the time scale for correlating transient response curves for the adsorbates and gaseous products involved in the reaction.

RESULTS

Pulse Reaction Studies

Figure 2a shows the MS rate profiles of the reactor effluent during the first two NO pulses over Cu–ZSM-5-83 in He at 673 K. IR spectra taken during the first NO pulse, synchronized with the MS time scale, is shown in Fig. 2b. The time scale of the effluent MS profiles was obtained by subtracting the time required for the effluent to travel from the IR cell to the MS from the actual time scale. The pulse profile, after being injected, broadens as it moves down the reactor system from the IR cell to the MS due to spreading of the NO pulse in He flow. As a result, the total time span for a single NO pulse obtained from the MS profiles is 4.5 times longer than that obtained for the IR spectra (Figs. 2a and 2b). Due to the lack of a gaseous species that can be clearly observed by both FTIR and MS, the time span for the FTIR and MS results was not adjusted. IR spectra of gaseous NO were included in Fig. 2 for comparison with the spectra of the NO adsorbate species.

Introduction of the NO pulse led to an increase in the NO, N_2O, and O_2 MS profiles as shown in Fig. 2a. The first NO pulse, equivalent to 40.14 μmol, produced 1.1 μmol of N_2O and 0.11 μmol of O_2. The QMG 112A MS exhibited a very low response factor for the species with an m/e ratio of 46, thus hampering the detection of NO_2. Temperature-programmed reaction (TPR) of 5% NO on Cu–ZSM-5 (33), however, produced a significant amount of NO_2 at 673 K, thus raising the possibility of NO_2 formation also under pulse reaction conditions at 673 K. The stoichiometric mass balance of the reactor inlet and outlet gaseous species for the NO pulse, obtained from the MS profiles, suggested the formation of 0.88 μmol of NO_2. NO decomposition on the Cu–ZSM-5-83 catalyst was accompanied by the formation of the following adsorbate species: NO^+, $Cu^{2+}(NO)$, $Cu^+(NO)$, and bridging $Cu^{2+}(NO_3^-)$ as shown in Fig. 2b. The bridging $Cu^{2+}(NO_3^-)$ species formed as well as disappeared later than all of the observed adsorbate species. Both NO pulses produced similar MS profiles and IR spectra. The MS profiles of both NO pulses revealed a lead–lag relationship during the elution of unreacted NO, formation of N_2O and O_2. O_2 formation lagged behind that of N_2O as well as the elution of unreacted NO.

Figure 3 shows the MS rate profiles of the reactor effluent during the first two NO pulses and the IR spectra during the first NO pulse over autoreduced Cu–ZSM-5-127 at 673 K. A NO pulse over Cu–ZSM-5-127 produced N_2

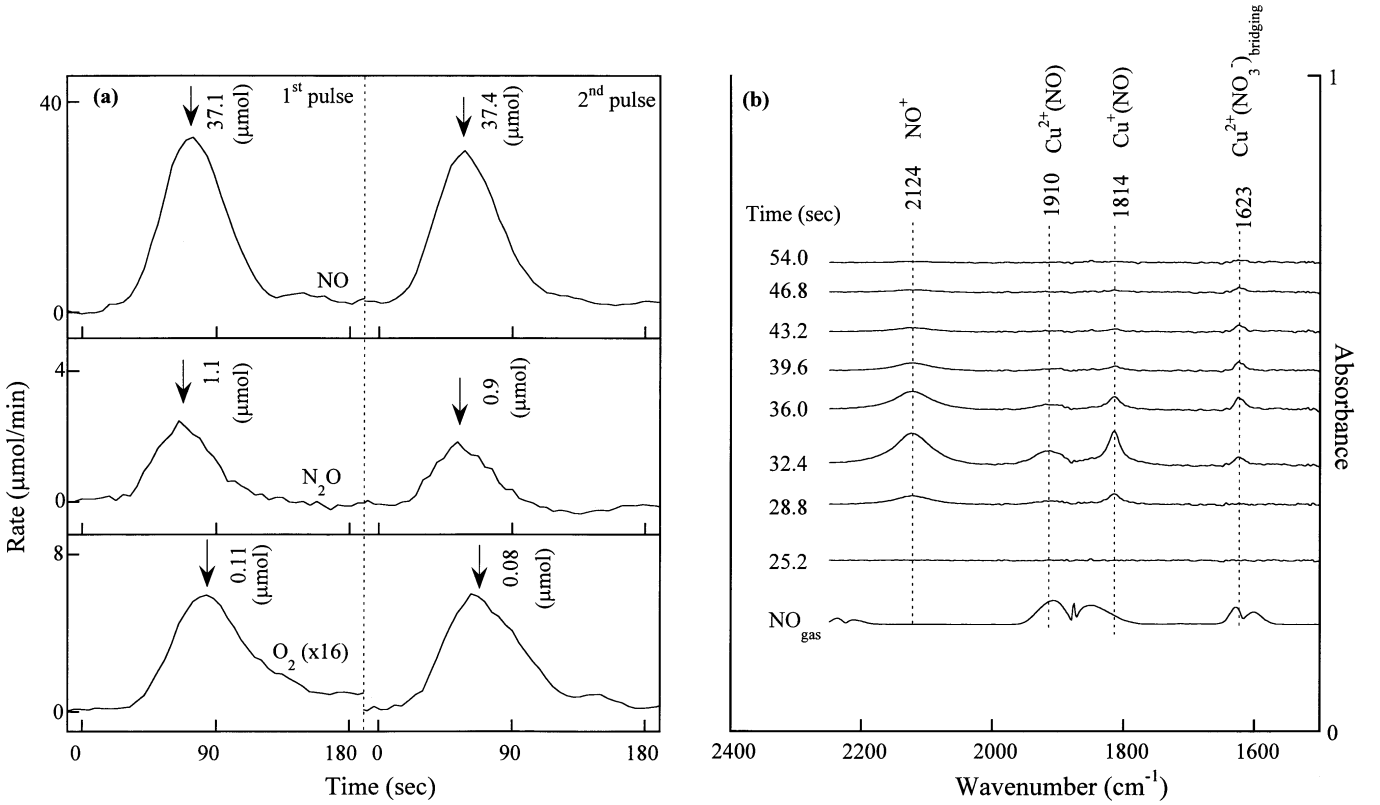

FIG. 2. (a) MS rate profiles of the reactor effluents during the 1st and 2nd 1 cm^3 of NO pulses in He and (b) FTIR rapid scan spectra during the 1st NO pulse, at 673 K over autoreduced Cu–ZSM-5-83.

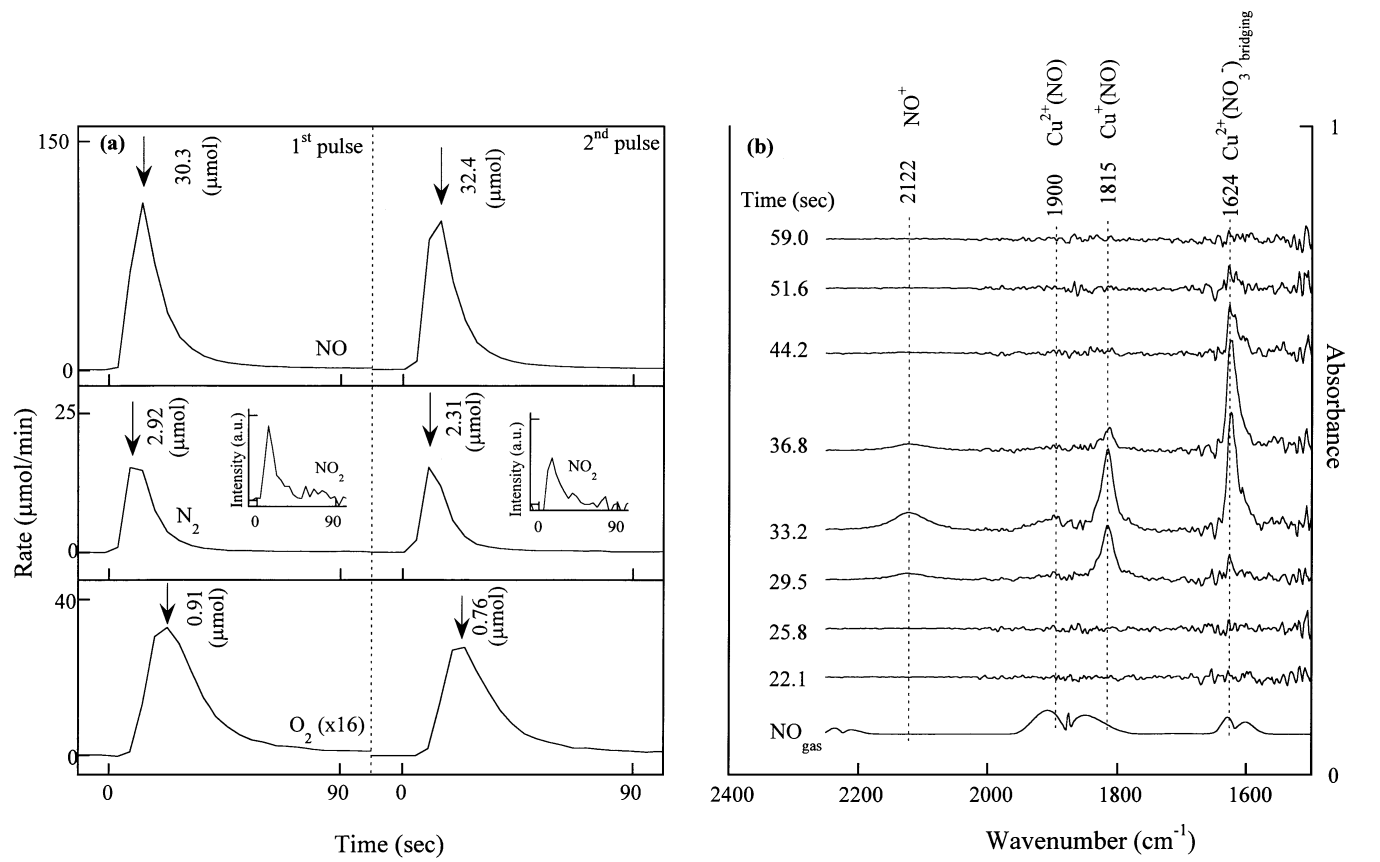

FIG. 3. (a) MS rate profiles of the reactor effluents during the 1st and 2nd 1 cm^3 of NO pulses in He and (b) FTIR rapid scan spectra during the 1st NO pulse, at 673 K over autoreduced Cu–ZSM-5-127.

TABLE 2

NO Conversion and Yields during Steady-State NO Flow (2.5 cm^3/min NO and 47.5 cm^3/min He) and Pulse NO (1 cm^3 into 47.5 cm^3/min He) Decomposition over Cu–ZSM-5-83 (0.101 g) and Cu–ZSM-5-127 (0.103 g) at 673 K

	Cu–ZSM-5-83		Cu–ZSM-5-127	
	Steady state	Pulse	Steady state	Pulse
		Conversion (%)		
NO	14.7 (2.4)[a]	7.2	21.1 (3.4)[a]	20.4
		Yields (%)		
$\frac{\text{moles of } N_2 \text{ produced}}{\text{moles of NO converted}}$	0	0	40.5	29.7
$\frac{\text{moles of } O_2 \text{ produced}}{\text{moles of NO converted}}$	0.2	3.4	3.7	9.5
$\frac{\text{moles of } N_2O \text{ produced}}{\text{moles of NO converted}}$	16.5	35.6	0	0
$\frac{\text{moles of } NO_2 \text{ produced}}{\text{moles of NO converted}}$	67.2	40.5	18.5	28.8

[a] Rate of NO conversion (μmol/s · g).

instead of N_2O and a greater amount of O_2 compared to the pulse over Cu–ZSM-5-83. The Prisma QMS 200 MS detected NO_2 formation. A comparison of NO conversion and yields during the NO pulse reaction over Cu–ZSM-5-83 and Cu–ZSM-5-127 at 673 K, listed in Table 2, shows that the over-exchanged catalyst exhibits higher NO conversion and higher O_2 yields than the under-exchanged Cu–ZSM-5. Conversion and yields of steady-state NO decomposition from our previous studies (33) are also listed in Table 2. The pulse reaction involved the exposure of the catalyst to a smaller quantity of the reactant (NO) for a shorter period of time; the steady state reaction involved the exposure of the catalyst to a continuous flow of the reactant. Despite a significant difference in NO conversion and yields, the pulse reaction on both under- and over-exchanged catalysts produced similar adsorbates in a similar sequence except high NO^+ and $Cu^{2+}(NO)$ intensities on Cu–ZSM-5-83 and high $Cu^+(NO)$ and bridging $Cu^{2+}(NO_3^-)$ intensities on Cu–ZSM-5-127.

Silane, Water, and Sulfur Dioxide Site Poisoning of Cu–ZSM-5

Figure 4 shows IR spectra of CO adsorption at 298 K followed by that of SiH_4 at the same temperature over autoreduced Cu–ZSM-5-83 and Cu–ZSM-5-127. CO adsorption produced $Cu^+(CO)_2$ at 2153 and 2177 cm^{-1} (13) on both the catalysts. Subsequent addition of gaseous SiH_4 produced the Si–H band at 2190 cm^{-1} over Cu–ZSM-5-83 and at 2210 cm^{-1}(31) over Cu–ZSM-5-127 in addition to the peak at 2153 cm^{-1}. Continued exposure to SiH_4 at 303 K caused a decrease in the intensity of (a) the OH bands in the 3600- to 3750-cm^{-1} region and H–O–H band at 1591 cm^{-1} over

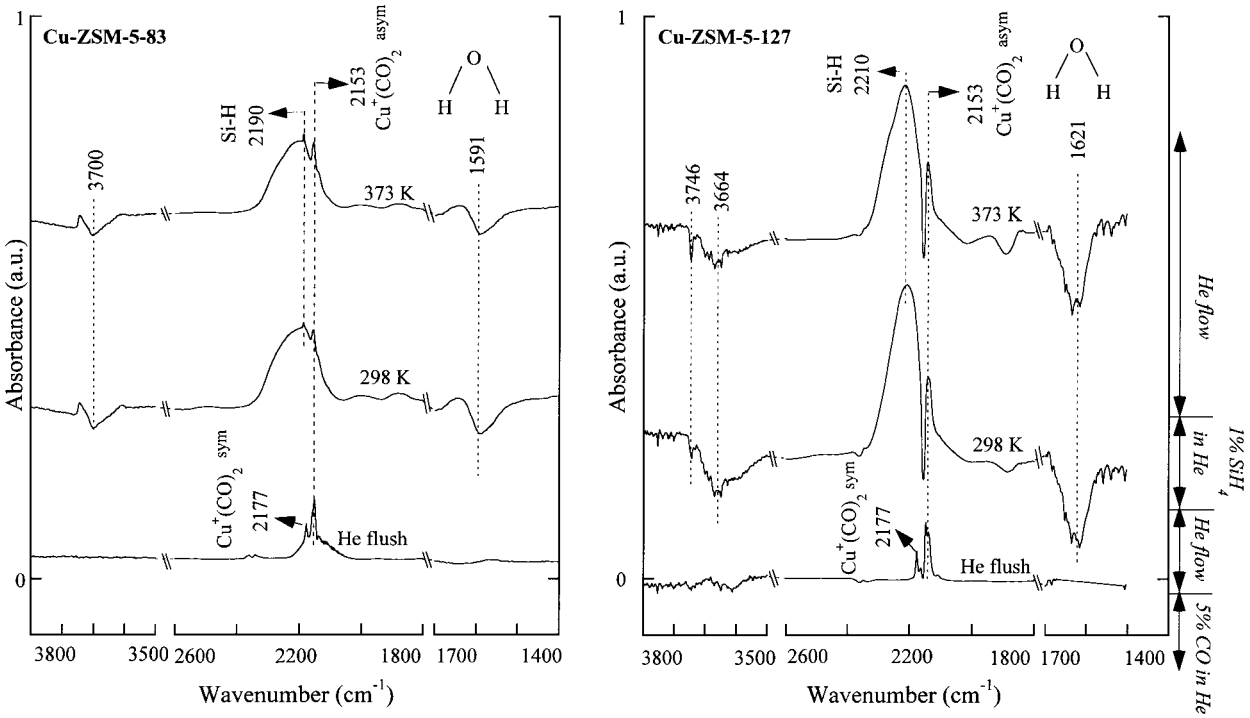

FIG. 4. FTIR spectra of (a) Cu–ZSM-5-83 and (b) Cu–ZSM-5-127 after flowing 5% CO and flushing with He at 298 K, 1% SiH_4 in He flow for 30 min at 298 K, subsequent He flush, and heating the catalyst to 373 K.

Cu–ZSM-5-83, (b) the OH groups in the 3600 to 3750 cm^{-1} region and H–O–H band at 1621 cm^{-1} over Cu–ZSM-5-127, and (c) little change in the $Cu^{+}(CO)_2$ intensity over both catalysts. Little variation in $Cu^{+}(CO)_2$ signified the absence of interaction of SiH_4 with the Cu^{+} species on the catalysts. A decrease in the OH band intensity in the 3600 to 3750 cm^{-1} region over both Cu–ZSM-5-83 and Cu–ZSM-5-127 indicates that SiH_4 reacts with the H of the –OH groups bonded to isolated silica sites, bonded by hydrogen bonding, and those present in the inside of the zeolite as shown below:

$$\text{–Si–OH} + SiH_4 \rightarrow \text{–Si–O–}SiH_3 + H_2.$$

Although Fig. 4 shows subtle differences in the interaction of the various hydroxyl groups with SiH_4, the present study does not provide an in-depth explanation of these interactions.

Exposure of both autoreduced catalysts (Cu–ZSM-5-83 and Cu–ZSM-5-127) to water produced –OH (3500–3600 cm^{-1}) and H–O–H (1620 cm^{-1}) characteristic bands in the IR spectra. Increasing the temperature to 773 K led to a decrease in the intensity of these bands and eventually led to their disappearance after exposure for 1 h. Traces of H_2O left in the IR cell were removed by flushing with He at 773 K.

Sulfur dioxide (0.1% SO_2 in N_2) exposure of the catalysts at 303 K did not cause a change in their IR spectra. S–O bands (1000–1200 cm^{-1}) could not be observed due to the low concentration of SO_2 and cutoff of IR radiation below 1200 cm^{-1} by the CaF_2 rods and windows used in the IR cell. The reactor was operated in the batch mode by heating to 373 K. Subsequently, SO_2 was flushed out of the IR cell by flowing He at 373 K.

Pulse Reaction Studies on Site-Poisoned Catalyst

Figure 5 compares the MS intensity profiles of the reactor effluents and IR spectra collected during the NO pulses over autoreduced (Figs. 5a and 5b), silane-treated (Figs. 5c and 5d), water-treated (Figs. 5e and 5f), and sulfur dioxide-treated (Figs. 5g and 5h) Cu–ZSM-5-83 at 673 K. Site poisoning decreased N_2O formation by a factor of 2 with silane and 2.5 with water and completely suppressed N_2O formation with sulfur dioxide; decreased O_2 formation by a factor of 4 with water and completely suppressed O_2 formation with silane and sulfur dioxide (Figs. 5a, 5c, 5e, and 5g). Infrared spectra show the consistent suppression of $Cu^{+}(NO)$ and bridging $Cu^{2+}(NO_3)^{-}$ species over all the site-poisoned catalysts (Figs. 5b, 5d, 5f, and 5h). Water treatment caused an increase in $Cu^{2+}O^{-}(NO)$ and sulfur dioxide treatment led to an increase of NO^{+}.

The MS intensity profiles of the reactor effluents and IR spectra collected during the NO pulses over autoreduced (Figs. 6a and 6b), silane-treated (Figs. 6c and 6d), water-treated (Figs. 6e and 6f), and sulfur dioxide-treated (Figs. 6g and 6h) Cu–ZSM-5-127 at 673 K are shown in Fig. 6. Similar to the under-exchanged Cu–ZSM-5, site poisoning of the over-exchanged catalyst decreased O_2 formation by a factor of 20 with water and completely suppressed O_2 formation with silane and sulfur dioxide. Site poisoning also decreased N_2 formation by a factor of 4.6 with silane and 5.8 with water and completely suppressed N_2 formation with sulfur dioxide (Figs. 6a, 6c, 6e, and 6g). Infrared spectra of Cu–ZSM-5-127 showed that site poisoning suppressed $Cu^{+}(NO)$ and bridging $Cu^{2+}(NO_3^{-})$ species over all the pretreated catalysts analogous to that over Cu–ZSM-5-83. Silane treatment also decreased the formation of NO^{+} species (Figs. 6b, 6d, 6f, and 6h). Table 3 shows the NO conversion and yields as

TABLE 3

NO Conversion and Yields (mol of Product/mol of Converted NO) for the 1 cm^3 of NO Pulses over Autoreduced and Pretreated Cu–ZSM-5-83 and Cu–ZSM-5-127 at 673 K; IR Band Intensities during the Pulse Reaction Studies over Site-Poisoned Catalysts

	Cu–ZSM-5-83				Cu–ZSM-5-127			
	Autoreduction	Water	Silane	Sulfur dioxide	Autoreduction	Water	Silane	Sulfur dioxide
				Conversion (%)				
NO	7.2	3.1	2.4	0.0	20.4	3.9	5.2	0.0
				Yield (%)				
N_2	0.0	0.0	0.0	0.0	29.7	26.2	25.0	0.0
O_2	3.4	2.2	0.0	0.0	9.5	2.3	0.0	0.0
N_2O	35.6	34.8	33.3	0.0	0.0	0.0	0.0	0.0
NO_2	40.5	30.3	33.3	0.0	28.8	47.6	50.0	0.0
				IR bands				
NO^{+}	Strong	Weak	Weak	Strong	Weak	Weak	Absent	Weak
$Cu^{+}(NO)$	Strong	Weak	Weak	Weak	Strong	Weak	Weak	Weak
$Cu^{2+}O^{-}(NO)$	Absent	Strong	Absent	Absent	Weak	Absent	Weak	Weak
$Cu^{2+}(NO)$	Strong	Absent	Strong	Strong	Absent	Weak	Absent	Absent
$Cu^{2+}(NO_3^{-})_{bridged}$	Strong	Absent	Absent	Absent	Strong	Absent	Absent	Absent

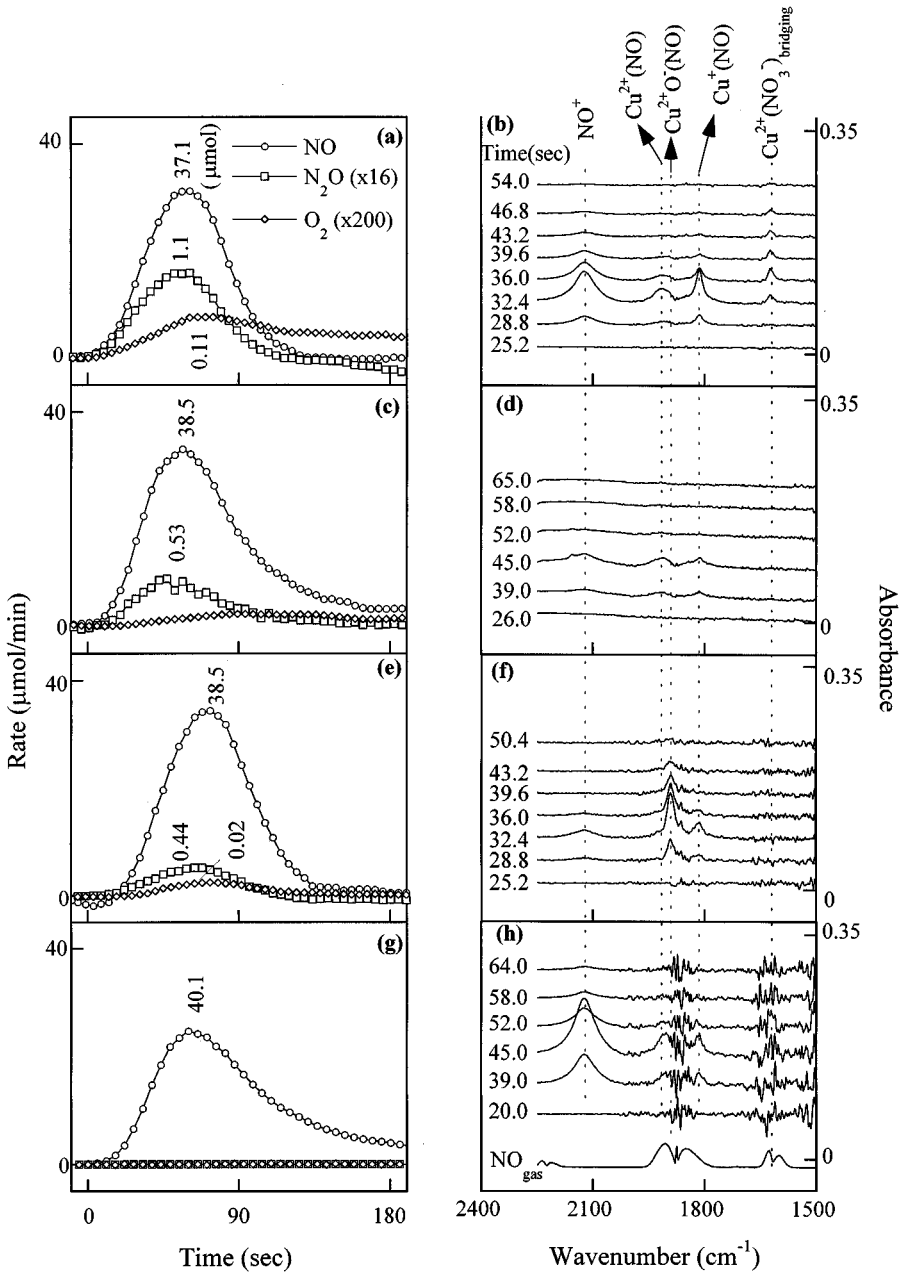

FIG. 5. MS intensity profiles of the reactor effluents during a 1 cm^3 of NO pulse over (a) autoreduced, (c) silane-treated, (e) water-treated, and (g) sulfur dioxide-treated Cu–ZSM-5-83; IR spectra collected during NO pulse over (b) autoreduced, (d) silane-treated, (f) water-treated, and (h) sulfur dioxide-treated Cu–ZSM-5-83 at 673 K.

well as variation in the IR intensity of adsorbates during the NO pulses over site-poisoned Cu–ZSM-5 catalysts at 673 K.

The Cu–ZSM-5-83 and Cu–ZSM-5-127 site-poisoned catalysts, exposed to NO pulse reaction studies at 673 K, were subsequently also subjected to similar pulse reaction studies at 723 and 773 K. Increases in temperature from 673 to 723 and 773 K did not change the rate of product formation.

Zeolite Analysis before/after Site-Poisoning and Pulse Studies

Figures 7 and 8 compare the transmission spectra, in the framework adsorption region, of autoreduced and silane-, water-, and sulfur dioxide-pretreated Cu–ZSM-5-83 and Cu–ZSM-5-127, respectively, under ambient conditions after the pulse studies. The transmission spectra were obtained by taking the ratio of (a) the spectrum of the pellet

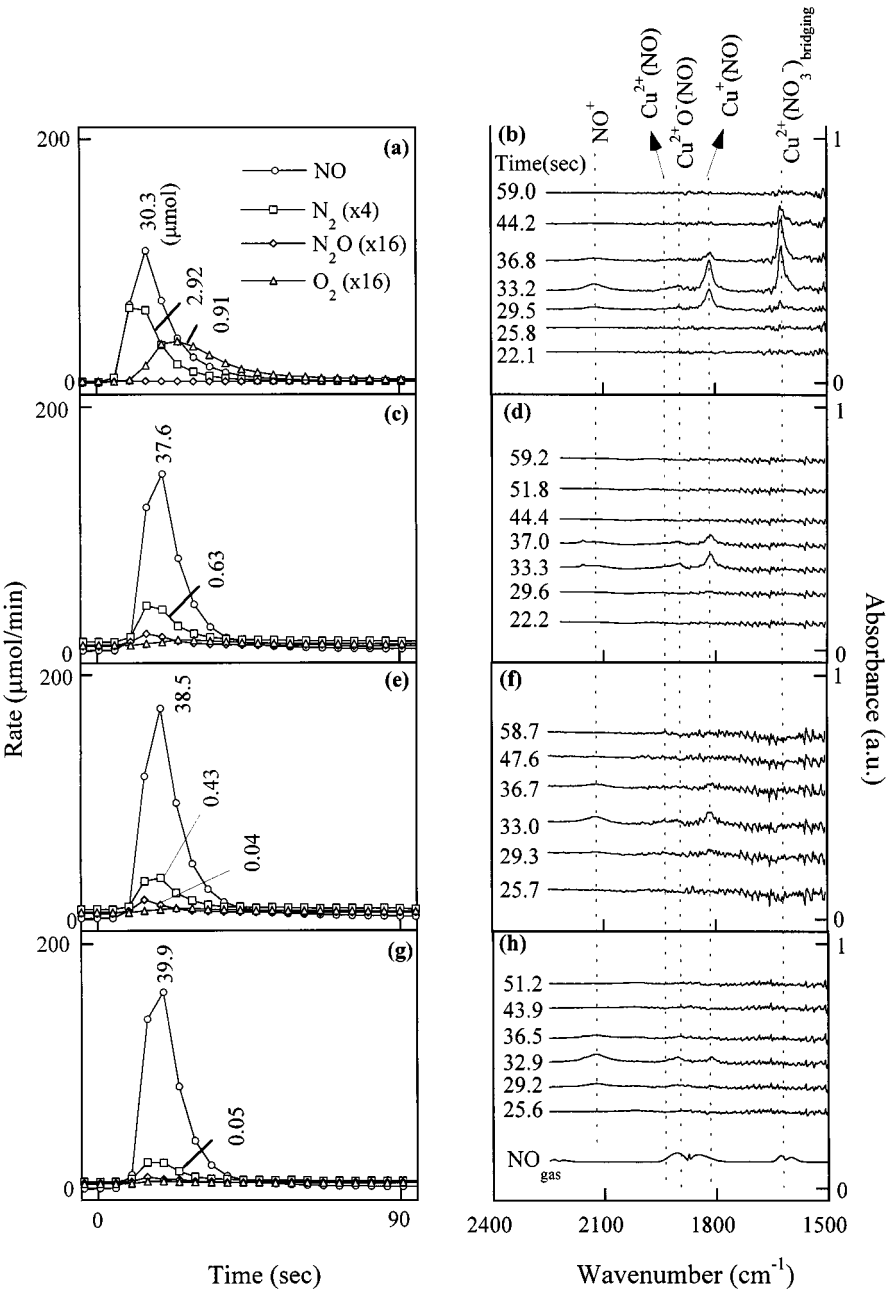

FIG. 6. MS intensity profiles of the reactor effluents during a 1 cm^3 of NO pulse over (a) autoreduced, (c) silane-treated, (e) water-treated, and (g) sulfur dioxide-treated Cu–ZSM-5-127; IR spectra collected during NO pulse over (b) autoreduced, (d) silane-treated, (f) water-treated, and (h) sulfur dioxide-treated Cu–ZSM-5-127 at 673 K.

obtained from a mixture of the catalyst and KBr and (b) the spectrum of the pellet obtained from KBr alone. The catalyst and KBr mixture was composed of 99.75% KBr and 0.25% Cu–ZSM-5 (0.5 mg of Cu–ZSM-5 in 200 mg of KBr). The pellet made from the autoreduced sample showed internal vibrations of the Si and AlO_4 tetrahedra at 1092 and 453 cm^{-1} and vibrations of the double-ring tetrahedra at 550 cm^{-1}. The position of the band at 550 cm^{-1} characterized the presence of a ZSM-5 framework in the zeolite (32). The intensity ratio of the 550- to 453-cm^{-1} bands was not affected by the NO pulse, as shown in Figs. 7 and 8, as well as by site poisoning, indicating that ZSM-5 maintained its framework during the site-poisoning and pulse reaction studies.

CO Pulse Studies

Figure 9 shows the MS profiles of the reactor effluent and Fig. 10a shows variation in the IR spectra during the

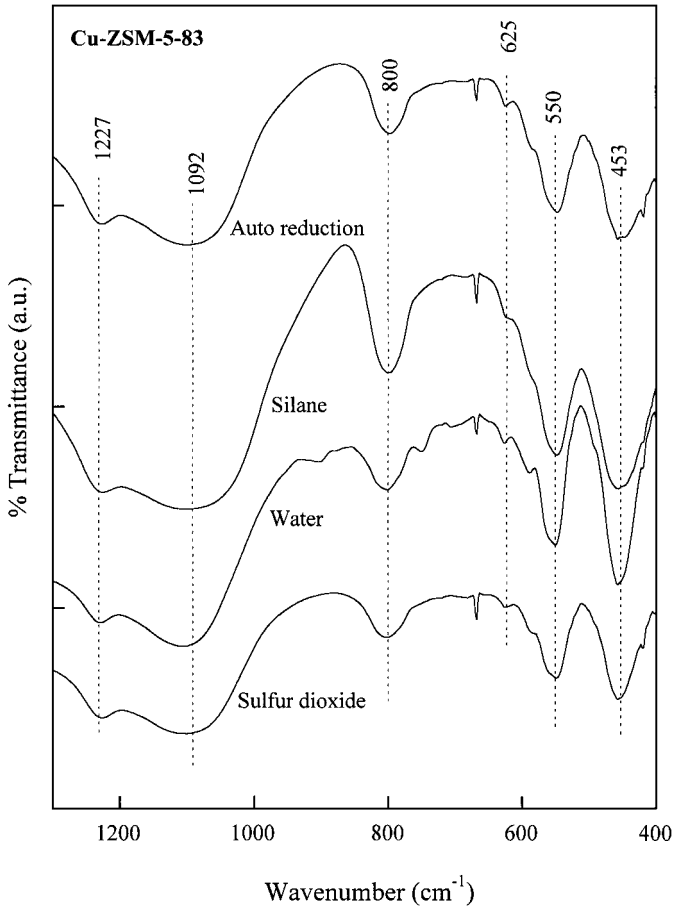

FIG. 7. FTIR transmission spectra of Cu–ZSM-5-83 after pretreatment by (a) autoreduction, (b) 1% silane, (c) water, and (d) 0.1% sulfur dioxide.

CO pulse into 5% NO in He flow over Cu–ZSM-5-127 at 673 K. The time scale of the MS profiles was modified by subtracting the time required for the effluent to travel from the IR cell to the MS from the actual time scale. Spreading of the MS and IR intensity profiles for the pulses, with respect to time, were accounted for by equating the time duration of $CO_{2(g)}$ (2359 cm^{-1}) obtained from the IR spectra to the time duration of CO_2 ($m/e = 44$) from the MS profiles. As a result, the time span for the MS profiles was divided by a factor of 3.8.

Exposure of Cu–ZSM-5-127 to 5% NO flow, prior to pulsing CO, resulted in the appearance of NO^+, $Cu^{2+}(NO)$, $Cu^+(NO)$, and bridging and chelating $Cu^{2+}(NO_3^-)$, as well as formation of N_2, N_2O, NO_2, and O_2. Introduction of the CO pulse decreased $Cu^+(NO)$, bridging and chelating $Cu^{2+}(NO_3^-)$, and NO_2 formation; led to the formation of new IR bands at 2109, 2157, and 2194 cm^{-1}; led to the formation of CO_2 (observed in the IR spectra and MS profiles); and increased O_2 and N_2O formation as well as NO conversion. Increases in the formation of N_2 and N_2O could not be confirmed as the MS profile of N_2 was monitored by the m/e ratio of 28 which was the same for CO while the MS profile of N_2O, monitored by the m/e ratio of 44, was the same for CO_2. Formation of CO_2 was, however, confirmed by the increase in the profile of the $m/e = 22$ species which is observed due to the double ionization of CO_2 (CO_2^{2+}). A separate study, using ^{13}CO, also shows a N_2, N_2O, and CO_2 formation rate increase upon the injection of ^{13}CO at 673–773 K (42).

Difference IR spectra show the presence of additional bands at 2141, 2147, 2152, 2159, 2165, and 2169 cm^{-1} during the CO pulse into 5% NO in He flow over Cu–ZSM-5-127 at 673 K, as displayed in Fig. 10b. The band at 2157–2159 cm^{-1} (Figs. 10a and 10b) can be assigned to $Cu^+(CO)$ (13, 17, 23, 35–36) while bands at 2165 (Fig. 10b) and 2194 cm^{-1} (Figs. 10a and 10b) can be assigned to the asymmetric and symmetric vibrations of $Cu^+(CO)_3$, respectively (17). Figure 10b also shows the presence of a single band at 2152 cm^{-1} which can be assigned to the asymmetric mode of $Cu^+(CO)_2$ (13, 17) whose symmetric mode, not observed, at 2176 cm^{-1} may be overlapping with that of $Cu^+(CO)_3$. The

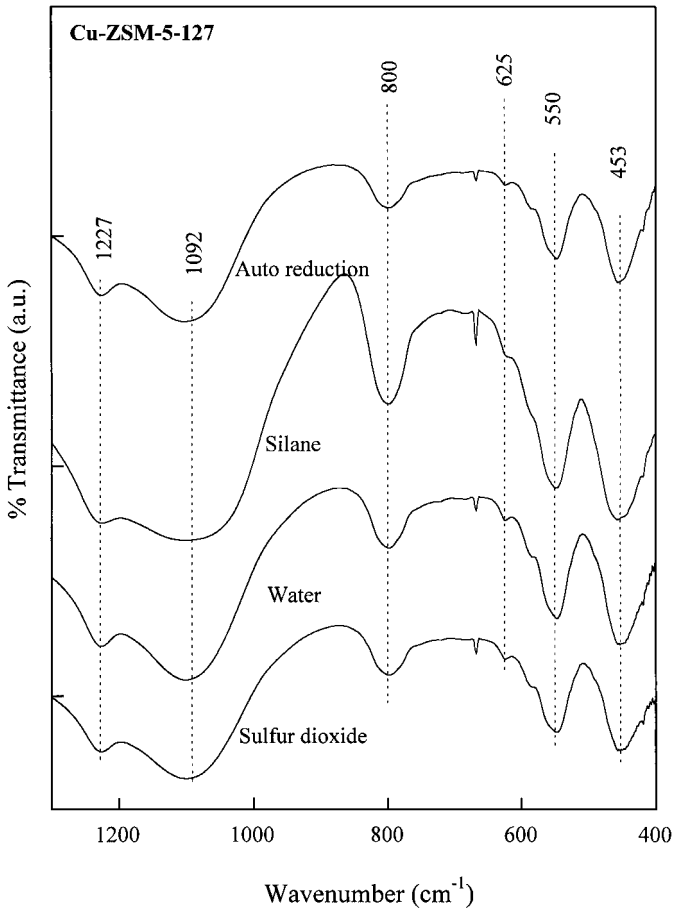

FIG. 8. FTIR transmission spectra of Cu–ZSM-5-127 after pretreatment by (a) autoreduction, (b) 1% silane, (c) water, and (d) 0.1% sulfur dioxide.

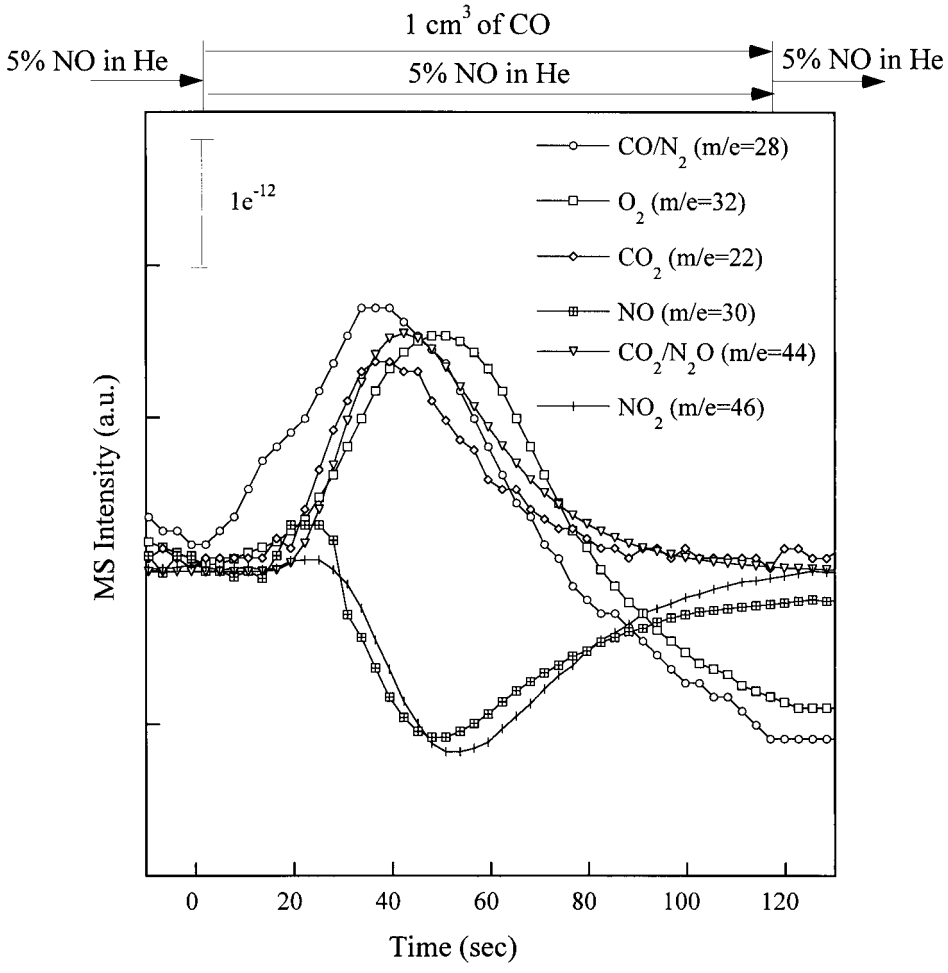

FIG. 9. MS intensity profiles during 1 cm^3 of CO pulse into 5% NO in He flow over Cu–ZSM-5-127 at 673 K.

band observed at 2109 cm^{-1} can be assigned to the adsorbed CO species bound on both sides to the Lewis acid center (13). Formation of $Cu^+(CO)_3$ in addition to $Cu^+(CO)$ and $Cu^+(CO)_2$ at 673 K in the presence of NO shows that CO adsorbs differently at 303 K (Fig. 4) and at 673 K under NO reaction conditions.

Variation of adsorbate and product concentration with time during the CO pulse is plotted in Fig. 11 to reveal the effect of CO on the Cu–ZSM-5 catalyst during NO decomposition. The rapid decay of $Cu^+(NO)$, bridging $Cu^{2+}(NO_3^-)$, and chelating $Cu^{2+}(NO_3^-)$ corresponded to a sharp increase in $Cu^+(CO)$, $Cu^+(CO)_3$, adsorbed CO, and gaseous CO_2 and O_2. An increase in the formation of O_2, which is indeed surprising, combined with the increase in adsorbed CO species on Cu^+ ($Cu^+(CO)$, $Cu^+(CO)_2$, and $Cu^+(CO)_3$) suggests that CO, the reducing agent, not only reduces Cu^{2+} to Cu^+ but also promotes desorption of oxygen. The depletion of $Cu^+(NO)$, bridging $Cu^{2+}(NO_3^-)$, and chelating $Cu^{2+}(NO_3^-)$ was accompanied by the increase of $Cu^+(CO)$, $Cu^+(CO)_3$, and adsorbed CO to a maximum. Ensuing the CO adsorbates reaching the maximum, CO_2 continued to rise and then decline; $Cu^+(CO)_3$ and adsorbed CO decayed corresponding to a symmetric increase of $Cu^+(NO)$; and $Cu^+(CO)$ began to decrease following the decrease of CO_2. The bridging and chelating $Cu^{2+}(NO_3^-)$ species began to emerge after all the adsorbed CO species were depleted.

DISCUSSION

Direct NO decomposition on the Cu–ZSM-5 catalyst has been studied extensively (10–22). However, few have reported the IR spectra of NO adsorbates on Cu–ZSM-5 exhibiting NO decomposition activity. The NO decomposition activity of Cu–ZSM-5 is sensitive to reaction conditions and dependent on copper loading and the Si/Al ratio. Hence, observations from separate adsorption and activity studies cannot be directly applicable to the identification of active adsorbates and formulation of a reaction pathway. The present study simultaneously measured the catalyst activity and dynamic behavior of the adsorbate species during the NO decomposition reaction under pulse reaction conditions on an autoreduced, site-poisoned, and CO-promoted

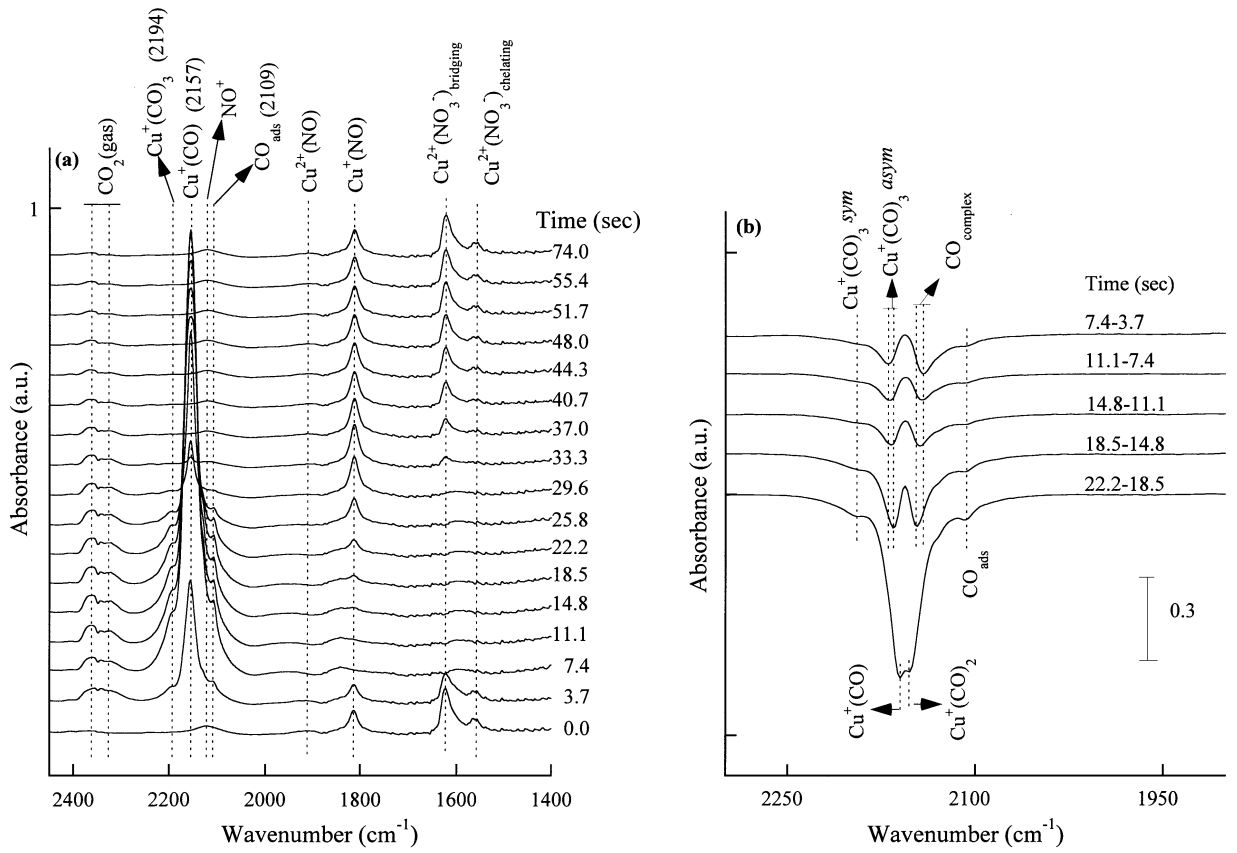

FIG. 10. (a) FTIR spectra and (b) difference FTIR spectra during 1 cm^3 of CO pulse into 5% NO in He flow over Cu–ZSM-5-127 at 673 K; difference spectra were obtained by subtracting the spectrum at a particular time and another at a different time, viz., the difference spectrum 7.4–3.7 was obtained by subtracting the spectrum at 3.7 s from that at 7.4 s.

Cu–ZSM-5 catalyst. Interpretation of adsorbate and reactant/product concentration profile results requires recognition of the facts that (i) adsorbate formation reflects the availability of sites to which the adsorbates are bound and (ii) an increase in the adsorbate profile indicates the rate of adsorbate formation being greater than its destruction (i.e., desorption or conversion to other species) rate.

Over- and Under-exchanged Cu–ZSM-5

Pulse and steady-state reaction studies (Table 2) show that over-exchanged Cu–ZSM-5 exhibits higher NO decomposition activity and higher N_2 selectivity than the under-exchanged catalyst. Cu–ZSM-5-83, however, exhibited higher N_2O selectivity compared to that of Cu–ZSM-5-127. The results are consistent with earlier reported studies (27, 40, 41). Despite differences in NO activity, N_2 and N_2O selectivity, the over- and under-exchanged Cu–ZSM-5 catalysts interact with NO to form the same IR-observable adsorbates and display similar adsorbate dynamics under reaction conditions (Figs. 2 and 3). The only difference was that $Cu^{2+}(NO_3^-)$ on Cu–ZSM-5-127 grew and decayed much faster than that on Cu–ZSM-5-127 during step reaction studies (33). The similarity in adsorbate structure and behavior over two catalysts with different activity and selectivity suggests that these IR-observable adsorbates may not participate in the rate-limiting step for reactant conversion and for product formation.

The adsorbate and reaction product profiles follow a sequence of formation during the pulse reaction (Figs. 2 and 3) and step switch reaction studies (33). $Cu^+(NO)$ and $Cu^{2+}(NO)$ precede the formation of bridging $Cu^{2+}(NO_3^-)$ while N_2/N_2O precedes that of O_2. The sequence of product and adsorbate formation allows postulation of the reaction pathways in Scheme 1.

Despite the lack of direct correlation between N_2O formation and intensity of $Cu^+(NO)$ on the under-exchanged Cu–ZSM-5 (Figs. 5a–5h), the N_2 formation rate appears to correlate with $Cu^+(NO)$ on the over-exchanged catalyst (Figs. 6a–6h). The close proximity in the evolution sequence of N_2 and N_2O with that of $Cu^+(NO)$ (Figs. 2 and 3) allows consideration of $Cu^+(NO)$ as not being directly involved, but as being in the path of NO dissociation and N_2 formation. In the event of $Cu^+(NO)$ being a direct precursor for N_2/N_2O formation, the concentration of reaction intermediates ($Cu^+(NO)$) preceding the products (N_2/N_2O) is

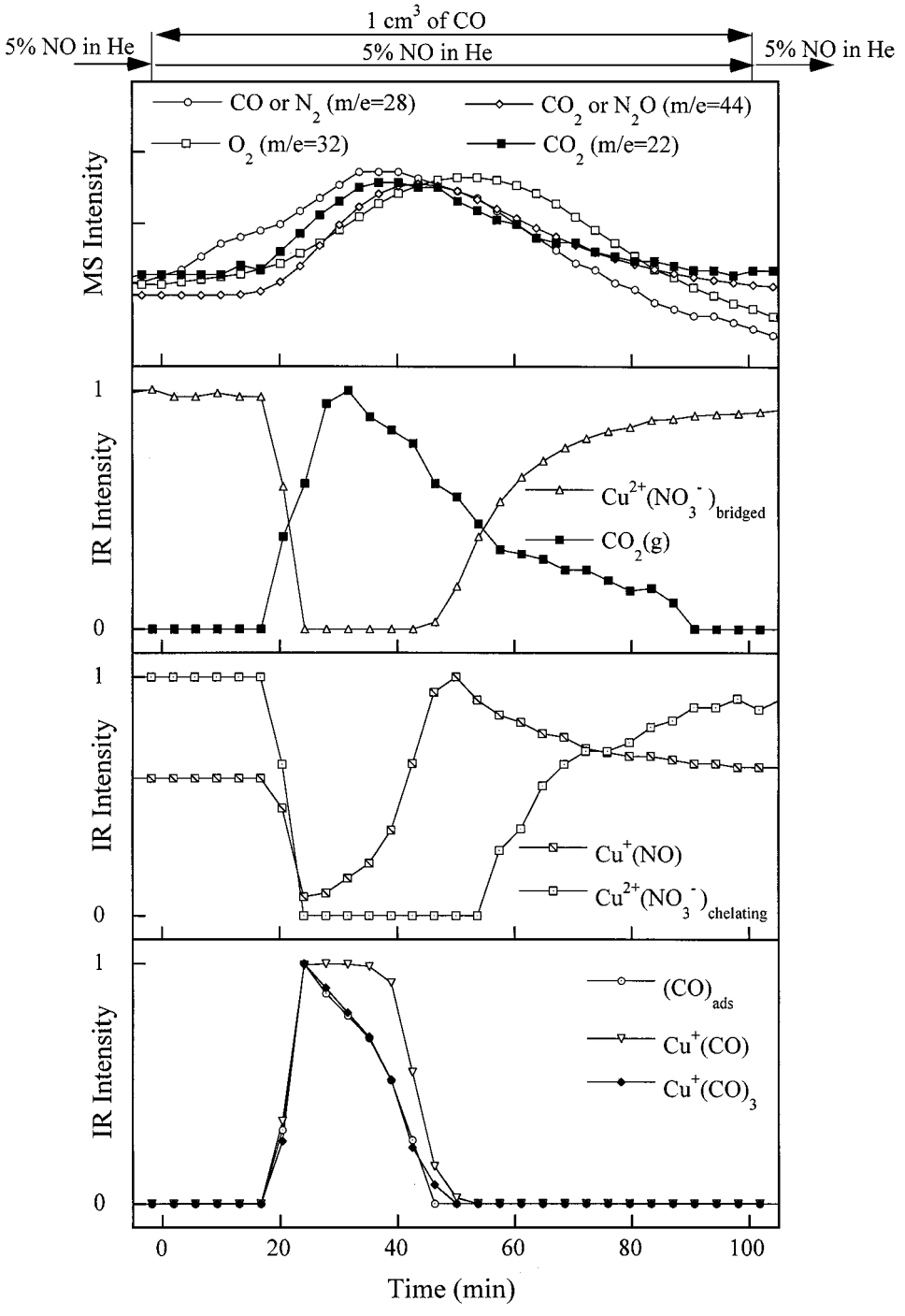

FIG. 11. Variation of MS and FTIR intensities during the 1 cm^3 of CO pulse into 5% NO in He flow over Cu–ZSM-5-127 at 673 K.

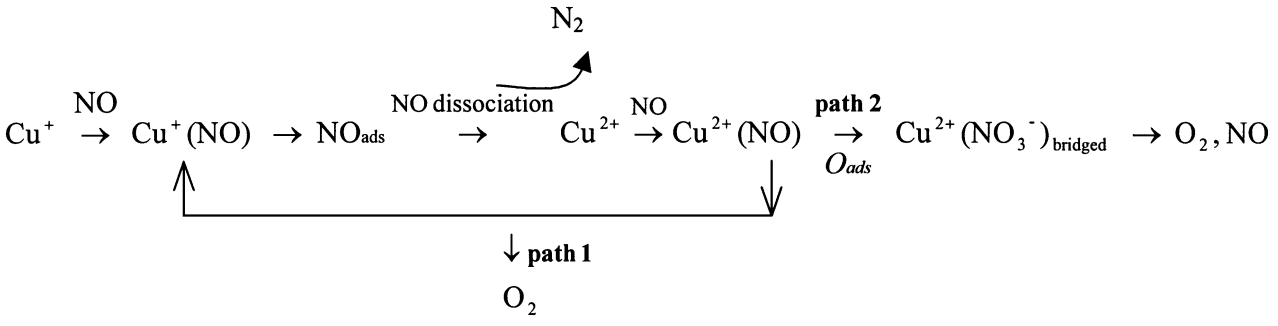

expected to decrease prior to an increase in the product concentration under pulse transient conditions. Since this is not the case, the supposition that $Cu^+(NO)$ is indirectly involved in N_2/N_2O formation is valid. $Cu^+(NO)$ could be a precursor for the formation of an intermediate species which in turn would be a precursor for NO dissociation. The reaction step involving the formation of such an intermediate cannot be detected by the IR/MS spectrometer reaction systems used in the present study. Therefore, NO_{ads} is arbitrarily placed in the reaction pathway, leading to NO dissociation as shown in Scheme 1.

One possible pathway (path 1) for O_2 formation is the autoreduction of Cu–ZSM-5 that reduces Cu^{2+} to Cu^+ and releases O_2. First principle quantum mechanical calculations (39) further supported the occurrence of path 1 by suggesting that Cu^{2+} species (CuO) reduced to Cu^+ producing O_2. The other pathway (path 2), involving $Cu^{2+}(NO_3^-)$, will be further elaborated in the following sections.

Site Poisoning and Promotion

The absence of O_2 and bridging $Cu^{2+}(NO_3^-)$ on the site-poisoned catalysts suggests that both O_2 and bridging $Cu^{2+}(NO_3^-)$ be produced from the same precursor whose formation has been inhibited by the poisoning. The formation of this precursor requires the migration of adsorbed oxygen available from the NO dissociation site that remains to be further investigated. Bridging $Cu^{2+}(NO_3^-)$ has been shown to decompose to N_2, NO, and O_2 under temperature-programmed reaction conditions (33). However, it is unclear whether bridging $Cu^{2+}(NO_3^-)$ would serve as a major precursor for O_2 formation under steady-state and pulse NO decomposition conditions.

Regardless of the proposed pathway (path 1 or 2), site poisoning by SiH_4, H_2O, and SO_2 inhibited bridging $Cu^{2+}(NO_3^-)$ and O_2 formation as well as autoreduction of Cu^{2+} to Cu^+. In contrast, N_2 and N_2O formation were suppressed to different extents, depending on the type of poisoning. The significant difference in the suppression of O_2 and N_2 formation brought about by site poisoning indicates that NO dissociation is not a common rate-limiting step for both N_2 and O_2 formation. The rate-limiting step for N_2 formation should be located between the final N_2 formation step and $Cu^+(NO)$ conversion step.

CO demonstrated effective reducing ability by immediately promoting the formation of CO_2, O_2, $Cu^+(CO)$, $Cu^+(CO)_2$, $Cu^+(CO)_3$, and adsorbed CO (Figs. 9 and 10). Although the increase in $m/e = 28$ does not allow the determination of variation in N_2 concentration in the reactor effluent, a separate ^{13}CO isotope pulse study shows that pulsing CO indeed increased the rate of N_2 formation (42). The absence of bridging $Cu^{2+}(NO_3^-)$ during the increase in O_2 formation demonstrated that bridging $Cu^{2+}(NO_3^-)$ is not the only precursor toward O_2 formation, further supporting the existence of a precursor and a pathway

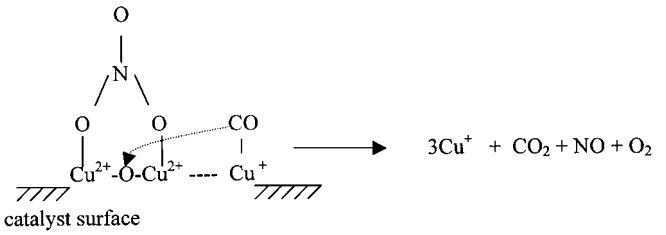

SCHEME 2

other than $Cu^{2+}(NO_3^-)$ for O_2 formation. This pathway, shown as path 1 in Scheme 1, that occurred during autoreduction could also take place during NO decomposition. The formation of O_2 and $Cu^+(CO)$ during the CO pulse also suggested that adsorbed CO reduced Cu^{2+} to Cu^+, facilitating the O–O combination. The symmetric profiles of $Cu^+(NO)$ and $Cu^+(CO)_3$ suggest that these two species share the same sites (Fig. 11). The greater delay of $Cu^{2+}(NO_3^-)$ behind $Cu^+(NO)$ during the CO pulse compared to the NO step/pulse NO shows that the lack of adsorbed O delayed the conversion of $Cu^+(NO)/Cu^{2+}(NO)$ to $Cu^{2+}(NO_3^-)$, since adsorbed O has been desorbed or reacted with CO to produce CO_2. The adsorbed O seems to be a requisite for $Cu^{2+}(NO_3^-)$ formation. The similar dynamics of the bridging and chelating $Cu^{2+}(NO_3^-)$ suggests that they may be in equilibrium (Fig. 11).

The depletion of bridging and chelating $Cu^{2+}(NO_3^-)$ as well as the formation of N_2O, CO_2, N_2, and O_2 upon addition of CO suggests the interaction of adsorbed CO with the nitrate species, leading to O_2 formation as shown in Scheme 2. It is suggested that CO from the $Cu^+(CO)$ species interacts with the O of Cu^{2+}–O–Cu^{2+} sites, producing CO_2, reducing Cu^{2+} to Cu^+, and decomposing the NO_3 species to NO and O_2. The interaction between adsorbed CO and the bridging nitrate species shown in Scheme 2 is not an elementary step as the reaction may be much more complex and is purely a speculative mechanism.

Reaction Mechanism

The NO decomposition reaction scheme (Scheme 1) can be further expanded into a detailed pathway that includes all the IR-observable adsorbates as shown in Fig. 12. NO adsorbs on the Cu^+ site to form $Cu^+(NO)$, as reported in earlier studies (13–19) and also shown in the present study in Figs. 2 and 3. NO dissociation has been envisioned to occur via three routes: (i) reaction of neighboring $Cu^+(NO)$ species alone or with $Cu^+(NO)_2$ to produce N_2/N_2O and $Cu^{2+}O$ (14); (ii) dissociation of $Cu^+(NO)_2$ to produce $Cu^{2+}O^-$ and N_2O (13, 15, 16); (iii) conversion of $Cu^+(NO)_2$ to $Cu^{2+}(N_2O_3^-)$ which dissociates to form N_2, N_2O, and O_2 (17, 19). Although $Cu^+(NO)_2$ has been proposed as a precursor for N_2O formation according to Cu(nitrosyl) chemistry (13, 15, 16), the lack of correlation between $Cu^+(NO)_2$

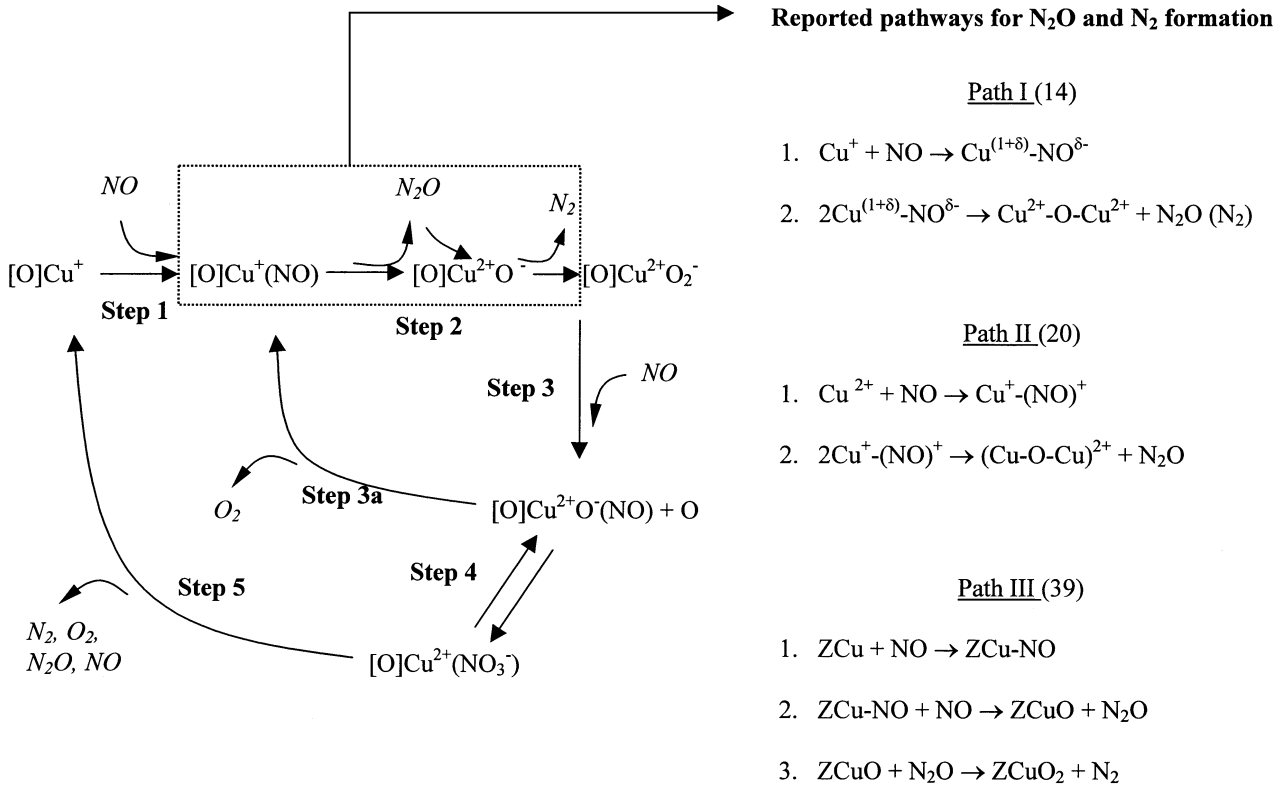

FIG. 12. Proposed NO decomposition reaction mechanism.

and N_2 formation (33) and first principles quantum mechanical calculations (39) suggest that $Cu^+(NO)_2$ is not formed under reaction conditions. Thus, $Cu^+(NO)_2$ as a precursor is ruled out. Results from the present IR studies suggest that the rate-limiting step for NO dissociation is located between $Cu^+(NO)$ and N_2 formation. The role of $Cu^+(NO)$ as a precursor for N_2O and N_2 formation has been reported earlier, as shown in path I–III (Fig. 12) (14, 20, 39).

The first two steps of path III can be used to explain the formation of N_2O on the under-exchanged Cu–ZSM-5 while the third step may explain N_2 formation on the over-exchanged Cu–ZSM-5. The lack of N_2O formation on over-exchanged Cu–ZSM-5 suggests that N_2O would not desorb from the surface to the gas phase and the lifetime of N_2O would be shorter than that detectable by the FTIR.

Subsequent NO adsorption on $Cu^{2+}O_2^-$ produced $Cu^{2+}O^-(NO)$ (step 3) whose presence during NO reaction conditions has been reported in the literature (13). The coordination and charge balance for the formation of $Cu^{2+}O_2^-$ remains to be investigated. O_2 formation beyond $Cu^{2+}O^-(NO)$ may proceed via (a) autoreduction of Cu^{2+} to Cu^+ to release O_2 (step 3a) and (b) the formation and subsequent decomposition of $Cu^{2+}(NO_3^-)$ to N_2, O_2, N_2O, and NO (steps 4 and 5). The O_2 formation steps are the most sensitive to surface modification. Even though Cu^+/Cu^{2+} were not modifed by silane, modification of the Cu^{2+}–O–Cu^{2+} site caused the inhibition of O_2 desorption/formation on the silane-poisoned Cu–ZSM-5.

Deactivation

Using Fig. 12 as the working NO decomposition mechanism, the susceptibility of each step in the pathway to site poisoning, on the basis of the effect of poison on adsorbate intensity and product amount, can be summarized as follows:

Step 1: Moderately poisoned by SiH_4 and slightly poisoned by SO_2 and H_2O on under-exchanged Cu–ZSM-5; moderately poisoned by SO_2 and slightly poisoned by H_2O and SiH_4 on over-exchanged Cu–ZSM-5.

Step 2: Moderately poisoned by SiH_4 and H_2O and completely poisoned by SO_2 on both the under- and over-exchanged Cu–ZSM-5.

Step 3a: Significantly poisoned by SiH_4, H_2O, and SO_2 on both the under- and over-exchanged Cu–ZSM-5.

Step 4: Completely poisoned by SiH_4, H_2O, and SO_2 on both the under- and over-exchanged Cu–ZSM-5.

Severe inhibition of O_2 formation by SiH_4, H_2O, and SO_2 poisoning shows that O_2 formation is the most fragile step. The presence of weak $Cu^+(NO)$ and $Cu^{2+}(NO)$ with near-complete suppression of bridging $Cu^{2+}(NO_3^-)$ and O_2 formation suggested that blocking of the Cu^+ and Cu^{2+} site

is not the major deactivation pathway for O_2 formation. Instead, inhibiting the migration of adsorbed oxygen for the formation of O_2 and bridging $Cu^{2+}(NO_3^-)$ is the dominant deactivation mechanism. A study of adsorbed oxygen on Cu–ZSM-5 is currently underway to reveal the oxygen formation pathway. The observation of N_2 and N_2O, even with a low rate of formation on the site-poisoned catalysts, shows that NO dissociation and N–N formation are more facile than O_2 formation and less severely inhibited by poisoning.

Spectator vs Active Adsorbates

Significant inhibition of NO^+ formation on SiH_4-poisoned Cu–ZSM-5 (Figs. 5d and 6d) and increase of NO^+ formation on SO_2-poisoned Cu–ZSM-5 (Figs. 5h and 6h) combined with the complete inhibition of O_2 formation (Figs. 5c, 5g, 6c, and 6g) indicates that the site on which NO^+ adsorbs does not play an active role in O_2 formation. Thus, NO^+ is a spectator adsorbate during the NO decomposition to N_2 and O_2.

$Cu^+(NO)$, though not a direct precursor, is in the pathway leading to N_2/N_2O formation; $Cu^{2+}(NO_3^-)$, always accompanied by O_2 formation, decomposes to N_2, O_2, N_2O, and NO during the NO decomposition reaction. Hence, $Cu^+(NO)$ and $Cu^{2+}(NO_3^-)$ are the active adsorbates for the NO decomposition reaction to N_2 and O_2 over Cu–ZSM-5.

SiH_4 Pretreatment

Our initial goal for SiH_4 treatment of Cu–ZSM-5 was to improve the catalyst hydrothermal stability by the removal of surface OH groups on ZSM-5. SiH_4 has been used as a precursor for the pore size modification of zeolites that also exhibited good thermal and water resistance (37, 38). The present study (Fig. 4) shows that SiH_4 reacts with and removes the surface hydroxyl group and also poisons NO decomposition activity. As a result, silanation cannot be used to improve hydrothermal stability of Cu–ZSM-5 for NO decomposition.

CONCLUSIONS

Direct NO decomposition reaction over Cu–ZSM-5 serves as a model reaction for the site-poisoning and -promotion technique. Site-poisoning and -promotion studies shed new light into the NO decomposition reaction mechanisms. The O_2 formation/desorption pathway proceeds via two routes: (a) autoreduction of Cu^{2+} to Cu^+ followed by desorption of O_2 and (b) decomposition of $Cu^{2+}(NO_3^-)$ to N_2, O_2, N_2O, and NO. $Cu^+(NO)$ and $Cu^{2+}(NO_3^-)$ act as active adsorbates while NO^+ acts as a spectator adsorbate during the NO decomposition to N_2 and O_2.

SiH_4 and H_2O severely poison O_2 formation but do not inhibit NO dissociation and N_2 formation. Inhibition of adsorbed O migration is the dominant deactivation pathway for O_2 formation/desorption rather than the blockage of Cu^+ and Cu^{2+} sites. Site promotion by CO addition enhances NO conversion and O_2 formation, suggesting the ability of a small amount of CO to promote NO decomposition.

ACKNOWLEDGMENT

Although the research described in this article has been funded entirely by the U.S. Environmental Protection Agency under assistance agreement R823529-01-0 to the University of Akron, it has not been subjected to the Agency's peer and administrative review and therefore may not necessarily reflect the views of the Agency and no official endorsement should be inferred.

REFERENCES

1. Tamaru, K., *in* "Catalysis: Science and Technology" (J. R. Anderson and M. Boudart, Eds.), Vol. 9, p. 87. Springer-Verlag, Berlin, Heidelberg, New York, 1991.
2. Delgass, W. N., Haller, G. L., Kellerman, R., and Lunsford, J. H., "Spectroscopy in Heterogeneous Catalysis." Academic Press, New York, 1979.
3. Srinivas, G., Chuang, S. S. C., and Debnath, S., *J. Catal.* **148**, 748 (1994).
4. Yamada, T., Onishi, T., and Tamaru, K., *Surf. Sci.* **157**, L389 (1985).
5. Lombardo, S. J., and Bell, A. T., *Surf. Sci.* **245**, 213 (1991).
6. Chuang, S. S. C., Krishnamurthy, R., and Tan, C. D., *Colloids Surf. A* **105**, 35 (1995).
7. Shido, T., and Iwasawa, Y., *J. Catal.* **141**, 71 (1993).
8. Akhter, S., and White, J. M., *J. Vac. Sci. Technol. A* **6**, 864 (1988).
9. Ceyer, C. T., *Langmuir* **6**, 82 (1990).
10. Iwamoto, M., Yoko, S., Sakai, K., and Kagawa, S., *J. Chem. Soc., Faraday Trans. 1* **77**, 1629 (1981).
11. Iwamoto, M., Furukawa, H., and Kagawa, S., *in* "New Developments in Zeolite Science and Technology" (Y. Murukama, A. Ichijima, and J. W. Ward, Eds.), p. 943. Elsevier, Amsterdam, 1986.
12. Li, Y., and Hall, W. K., *J. Phys. Chem.* **94**, 6145 (1990).
13. Aylor, A. W., Larsen, S. C., Reimer, J. A., and Bell, A. T., *J. Catal.* **157**, 592 (1995).
14. Iwamoto, M., Yahiro, H., Mizuno, N., Zhang, W.-X., Mine, Y., Furukawa, H., and Kagawa, S., *J. Phys. Chem.* **96**, 9360 (1992).
15. Giamello, E., Murphy, D., Magnacca, G., Morterra, C., Shioya, Y., Nomura, T., and Anpo, M., *J. Catal.* **136**, 510 (1992).
16. Valyon, J., and Hall, W. K., *in* "Proceedings of the 10th International Congress on Catalysis, Budapest, 1992" (L. Guczi, F. Solymosi, and P. Tetenyi, Eds.), p. 1341. Akademiai Kiado, Budapest, 1993.
17. Spoto, G., Zecchina, A., Bordiga, S., Ricchiardi, G., Marta, G., Leofanti, G., and Petrini, G., *Appl. Catal. B* **3**, 151 (1994).
18. Hoost, T. B., Laframboise, K. A., and Otto, K., *Catal. Lett.* **33**, 105 (1995).
19. Cheung, T., Bhargava, S. K., Hobday, M., and Foger, K., *J. Catal.* **158**, 301 (1996).
20. Adelman, B. J., Beutel, T., Lei, G.-D., and Sachtler, W. M. H., *J. Catal.* **158**, 327 (1996).
21. Hadjiivanov, K., Saussey, J., Freysz, J. L., and Lavalley, J. C., *Catal. Lett.* **52**, 103 (1998).
22. Jang, H.-J., Hall, W. K., and d'Itri, J. L., *J. Phys. Chem.* **100**, 9416 (1996).
23. Nakamoto, K., Fujita, J., and Murata, H., *J. Am. Chem. Soc.* **80**, 4817 (1958).
24. Cleare, M. J., and Griffith, W. P., *J. Chem. Soc. A* 1144 (1967).

25. Pozdnyakov, D. V., and Filiminov, V. N., *Kinet. Catal.* **14**, 655 (1973).
26. Addison, C. C., and Gatehouse, B. M., *J. Chem. Soc.* 613 (1960).
27. Iwamoto, M., Yahiro, H., Tanda, K., Mizuno, N., Mine, Y., and Kagawa, S., *J. Phys. Chem.* **95**, 3727 (1991).
28. Leyden, D. E., "Silanes, Surfaces, and Interfaces." Gordon and Breach, New York, 1985.
29. Chuang, S. S. C., and Lopez, B., *in* "Progress in Zeolite and Microporous Materials" (H. Chon, S.-K. Ihm, and Y. S. Uh, Eds.), Studies in Surface Science and Catalysis, Vol. 105, p. 1477. 1995.
30. Chuang, S. S. C., Brundage, M. A., Balakos, M., and Srinivas, G., *Appl. Spectrosc.* **49**(8), 1151 (1995).
31. Silverstein, R. M., Bassler, G. C., and Morrill, T. C., "Spectrometric Identification of Organic Compounds," p. 130. John Wiley and Sons, New York, 1991.
32. Coudurier, G., Naccache, C., and Vedrine, J. C., *J. Chem. Soc., Chem. Commun.* 1413 (1982).
33. Konduru, M. V., and Chuang, S. S. C., *J. Phys. Chem.* **103**, 5802 (1999).
34. Levenspiel, O., "Chemical Reaction Engineering," pp. 293–296. John Wiley and Sons, New York, 1999.
35. Hadjiivanov, K., Klissurski, D., Ramis, G., and Busca, G., *Appl. Catal. B* **7**, 251 (1996).
36. Yamashita, H., Matsuoka, M., Tsuji, K., Shioya, Y., Anpo, M., and Che, M., *J. Phys. Chem.* **100**, 397 (1996).
37. Thijs, A., Peeters, G., Vansant, E. F., and Verhaert, I., *J. Chem. Soc., Faraday Trans.* **79**, 2821 (1983).
38. Choplin, A., *J. Mol. Catal.* **86**, 501 (1994).
39. Trout, B. L., Chakraborty, A. K., and Bell, A. T., *J. Phys. Chem.* **100**, 17582 (1996).
40. Pirone, R., Giambelli, P., Moretti, G., and Russo, G., *Appl. Catal. B* **8**, 197 (1996).
41. Li, Y., and Hall, W. K., *J. Catal.* **129**, 202 (1991).
42. Konduru, M. V., Ph.D. preliminary research, The University of Akron, 1999.